

## CORONAS-F observation of HXR and gamma-ray emissions from the solar flare X10 on 29 October 2003 as a probe of accelerated proton spectrum

V.G. Kurt<sup>1</sup>, B.Yu. Yushkov<sup>1</sup>, K. Kudela<sup>2</sup>, V.I. Galkin<sup>1,3</sup> and L.K. Kashapova<sup>4</sup>

<sup>1</sup> *Skobeltsyn Institute of Nuclear Physics, Lomonosov Moscow State University, Moscow, 119991, Russia*

<sup>2</sup> *Institute of Experimental Physics, Slovak Academy of Sciences, Košice, 04001, Slovakia*

<sup>3</sup> *Faculty of Physics, Lomonosov Moscow State University, Moscow, 119991, Russia*

<sup>4</sup> *Institute of Solar-Terrestrial Physics, Russian Academy of Sciences, Irkutsk, 664033, Russia*

Received: January 29, 2015; Accepted: April 6, 2015

**Abstract.** HXR and gamma-ray emissions in the 0.04–150 MeV energy range associated with the solar flare on 29 October 2003 (X10/3B) were observed at 20:38–20:58 UT by the SONG instrument aboard the CORONAS-F mission. We restored consecutive flare gamma-emission spectra from SONG and RHESSI data and found a good agreement of these spectra in the 0.1–10 MeV energy range. Two phases were identified which showed major changes in the spectral shape of flare emission: 20:38:00–20:44:20 UT and 20:44:20–20:58:00 UT. During the second phase an efficiency of proton acceleration increased considerably relatively to the efficiency of acceleration of high energy electrons. The pion-decay component of the flare gamma-emission was elicited statistically significant only during the second phase since 20:47:40 UT. A power law spectrum index of accelerated protons was estimated from the ratio between intensities of the pion-decay and gamma-line components. The hardest spectrum (power law index  $S=3.7$ ) was at 20:48–20:51 UT when the intensity of the pion-decay emission was maximal. Our subdivision of the flare into two phases is consistent with sharp changes in the structure of the flare found by Ji et al. (2008) and Liu et al. (2009).

This flare was accompanied by GLE 66. The time profile of the pion-decay gamma-emission was compared with the GLE onset time. It was shown that both protons interacting at the Sun and the particles responsible for the GLE onset could belong to the same population of accelerated particles.

**Key words:** solar flares – acceleration of particles – X-rays, gamma-rays – pion-decay emission

## 1. Introduction

It is generally accepted that the energy of a flare is a magnetic energy accumulated in the solar corona. During the flare this energy converts into energy of accelerated particles, motion of matter, heat and shock waves. Processes of particle acceleration up to relativistic energies during solar flares can be studied through observations of hard X-ray (HXR) and gamma-ray emissions. This is especially the case with acceleration of relativistic electrons and high-energy protons. The time of ion acceleration up to high energies during an energetic eruption is one of open questions in solar physics, because both flares and CMEs can be potential sources of particle acceleration. Interest in this problem is caused, in particular, by the fact that high-energy protons escaping the Sun can produce Ground Level Enhancements (GLEs).

Accelerated electrons, depending on their pitch angles, can be trapped in the corona or precipitate into the chromosphere. Trapped electrons generate gyrosynchrotron/synchrotron radiation observed as a substantial amount of radio waves, down to millimeter and sub-millimeter bands. Precipitating electrons produce bremsstrahlung HXR and/or gamma-ray continuum with energies up to those of electrons themselves, and this bremsstrahlung spectrum is determined unambiguously by the electron spectrum (Miller and Ramaty, 1989). These electrons heat the chromospheric plasma. The hot material moves upward filling flare loops, which begin to emit the soft X-rays (SXR). There is a qualitative relationship between HXR (20-100 keV) and positive portion of SXR - the Neupert effect (Neupert, 1968; Hudson, 1991; Dennis and Zarro, 1993). This empirical relation implies that electrons contribute the greater part of the energy to the volume emitting SXR (e.g., Hudson, 1991; Dennis et al., 2003). So HXR emission and/or the derivative of SXR radiation -  $dI_{SXR}/dt$  act as an indicator of the electron acceleration rate, and are usually considered to be an observable manifestation of the flare energy release.

Protons accelerated to energies of tens of MeV excite nuclei of ambient matter, and these nuclei emit gamma-lines in the 0.5–12 MeV energy range (Ramaty and Murphy, 1987; Murphy et al., 2009). If protons gain energies above 300 MeV, they can produce neutral and charged pions through interactions with the solar atmosphere matter. These pions, in turn, decay and generate gamma-ray emission with a specific spectrum, namely a broad plateau in the 30–150 MeV energy range (e.g., Murphy et al., 1987; Ramaty and Murphy, 1987).

The list of solar flares with reliably identified pion-decay emission during flare impulsive phase is very short. The first flare with convincing evidence of pion-decay production was observed by the Gamma-Ray Spectrometer (GRS) of the Solar Maximum Mission (SMM) on 1982 June 3 (Forrest et al., 1985; 1986; Chupp et al., 1987). Recently, the pion-decay emission was detected in several experiments – SMM/GRS (Dunphy et al., 1990; 1991; Vestrand et al., 1999), GRANAT/Phebus (Debrunner et al., 1997; Vilmer, 1994; Terekhov et al., 1996), Compton GRO (Schneid et al., 1996; Dunphy et al., 1999; Rank et

al., 2001), and GAMMA/GAMMA1 (Akimov et al., 1991; 1996). A brief review of all above observations can be found in Chupp et al. (2003 and 2009). This emission was also detected during the declining phase of the solar cycle 23 by the Solar Neutrons and Gamma-rays (SONG) spectrometer (Kuznetsov et al. 2004) on the Complex Orbital Observations of the Active Sun (CORONAS-F) space mission from four solar flares (Kurt et al., 2010a, 2013a; Kuznetsov et al., 2011). A brief review of all above observations can be found in (Chupp et al., 2003 and 2009). This emission was also detected in several flares during the current solar activity cycle by Fermi with the Large Area Telescope (LAT) having very high sensitivity (Ackermann et al. 2012; 2014).

Even in some of the first observed flares (1982 June 3 and 1990 May 24) it was shown that the rise time of high-energy gamma-rays can be very short - of an order of ten seconds. It means that ions can be accelerated during the flare impulsive phase to relativistic energies in such a short time (Forrest et al., 1986; Debrunner et al., 1997). Nevertheless, there are two events, also observed by the SMM/GRS detector: 1988 December 16 (Dunphy et al., 1990; Alexander et al., 1994), and 1989 March 6 (Dunphy et al., 1991; Marschhäuser et al., 1991; Rieger and Marschhäuser, 1991; Alexander et al., 1994) and the 1991 June 11 flare observed aboard the Compton GRO by the COMPTEL and EGRET instruments (Dunphy et al., 1999; Rank et al., 2001) that exhibited several single emission pulses separated by a few minutes. The pion-decay component in these flares was reliably identified only a few minutes after the first, strongest episode of the energy release, and recorded afterwards for a long time. Thus, questions were raised how acceleration of particles to high energy is related to general development of each flare. Answers to these questions have not been found yet. Therefore, an increase in the number of the events with pion-decay emission measurements is very important (see, for example, reviews by Chupp et al., 2003; 2009; Vilmer et al., 2011).

This flare was also observed by the Transition Region and Coronal Explorer (TRACE) in the UV wavelength and by the Ramaty High Energy Solar Spectroscopic Imager (RHESSI) in HXR and gamma-ray energy range up to 10 MeV. In the unique paper, Hurford et al. (2006) carried out comparison of imaged and spatially integrated fluences in the 2.223 MeV gamma-line of this flare and showed that most, if not all, of the emission was confined to compact sources (with size scales of tens of arc seconds or smaller) located within the flare active region. Thus, the authors concluded that the gamma-ray-producing ions with 10-50 MeV energies “appear to be accelerated by the flare process and not by a widespread shock driven by a fast coronal mass ejection”.

A lot of publications based on the RHESSI data deal mostly with a photon energy range from 6 to 150 keV. These studies investigated the magnetic field spatial structure variations during the flare. Complete coverage of this flare and the high cadence TRACE 1600Å Michelson Doppler Imager (MDI) magnetogram, combined with RHESSI HXR observations, allowed to find two distinct phases of HXR kernel motion, two arcade systems with different magnetic shear

and two peaks of the calculated reconnected electric field in these phases of the flare (Ji et al., 2008; Zhou et al., 2008; Liu et al., 2009; Hu et al., 2010; Yang et al., 2011). Thanks to these publications we have got an opportunity to compare the dependence of proton acceleration efficiency to high energies with conspicuous changes in the structure of the flare region.

The goal of the present study was to refine the onset time of the efficient acceleration of high-energy protons on the time scale of the 29 October 2003 GOES class X10 flare (W05 S18) observed with CORONAS/SONG in the energy range of 0.04–150 MeV. These observations lasted 20 minutes and covered the whole flare impulsive phase that provided the opportunity to trace the time evolution of the emission spectrum and find the time of appearance of the pion-decay component.

This flare was accompanied by GLE 66. We compared time profiles of the pion-decay gamma-emission and the GLE in order to answer the question: do particles producing the pion-decay emission and particles responsible for the GLE onset belong to the same population of accelerated particles?

## 2. CORONAS-F SONG observations

To study the neutral emissions from solar flares (HXR and gamma-ray emission in the 40 keV–300 MeV energy range), as well as neutron and relativistic electron fluxes, the SONG detector has been designed by the Skobeltsyn Institute of Nuclear Physics, Lomonosov Moscow State University, in collaboration with the Institute of Experimental Physics, Slovak Academy of Sciences (Kuznetsov et al, 2004; 2011). It was installed aboard the CORONAS-F mission. The SONG instrument had a CsI crystal with a diameter of 20 cm and a height of 10 cm as the main detecting element. The crystal was surrounded by an anticoincidence plastic scintillator shield to reject signals from charged particles. A brief description of the SONG was presented by Kuznetsov et al. (2011); the latter paper also contains the description of the in-flight-calibration procedure and the background subtraction routine.

The 29 October 2003 flare was observed by CORONAS-F under favorable conditions – near the equator region where the background level was low that allowed us to distinguish a faint excess above the background of count rates in the high-energy channels. Figure 1 shows the response of the SONG detector to the flare HXR and gamma emissions over the range of energy losses from 0.04 to 150 MeV. The net count rates due to the flare (4-s time bins) were obtained by subtracting the background count rates. Count rates above 6 MeV were accumulated in 40-second bins to improve poor statistics. We demonstrate also other observational manifestations of this flare to indicate the context for our detailed discussion and to follow spectral evolution of high-energy emissions.

To obtain the flare morphology we focused firstly on the 20:38–20:58 UT time interval visible in the HXR/gamma-emission time profile up to the channel 10.5

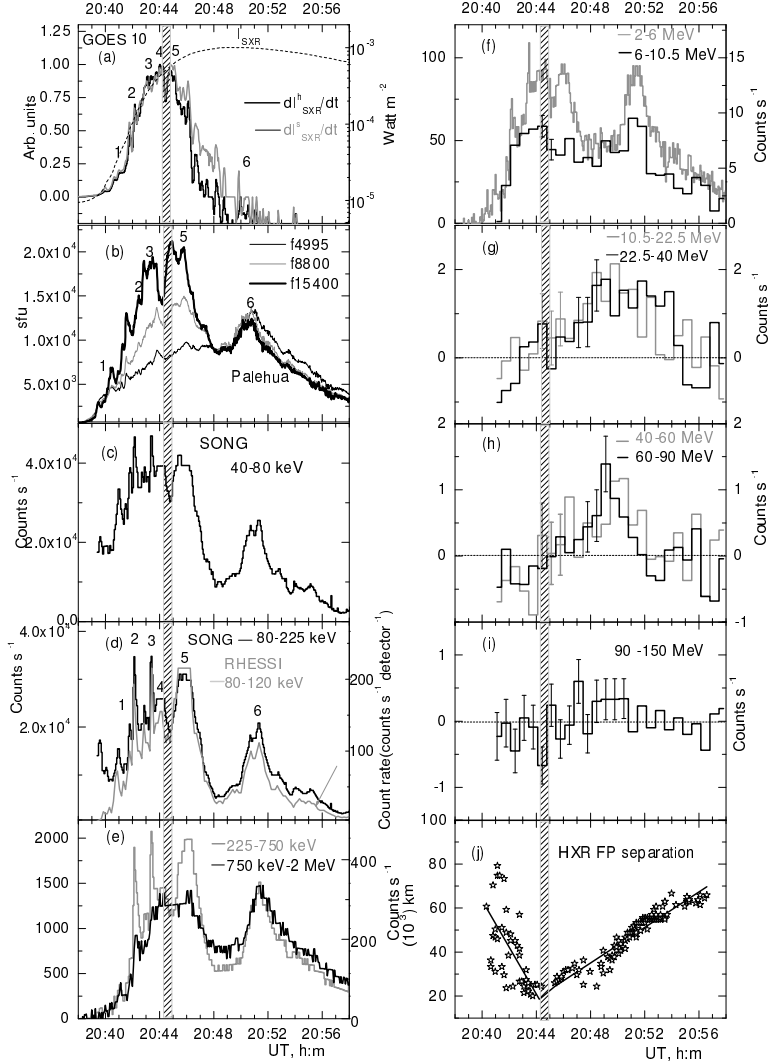


**Figure 1.** A GOES SXR light curve and derivative – (a); light curves of Palehua radio emission at three frequencies – (b). Next panels – time histories of the SONG response during 29 October 2003 flare – (c-i). Gray line on panel (d) – the RHESSI light curve in 80-120 keV energy range (right axes) The RHESSI fluxes are average count rates of front segments 1, 3–6, 8, and 9 with contamination from radiation belt particles removed (Liu, 2009). The right Y axis in panels e and f corresponds to SONG higher energy channels. The panel (k) represents time dependence of FP separation measured in 70-150 keV energy range and linear fits of FP velocities. This graph was taken from Fig.1 of panel b, Ji et al., 2008. The time when FPs stopped converging and began to move away from each other is denoted by the vertical sparse area.

MeV and in the radio burst. It is possible to distinguish several individual spikes numbered as 1-6 in the panels (a, b, d). Spikes 4 and 5 can be isolated only in several emissions. Spike 5 is separated from spike 6 by quite a broad intermediate time interval with the decreasing intensity of radio emission at 8.8 and 15.4 GHz and the count rate in the SONG low-energy channels from 40-80 keV up to 2-6 MeV. Such temporal behavior of the HXR intensity can be seen in the RHESSI data (panel d).

$dI_{SXR}/dt$  is usually considered as a qualitative indicator of the flare energy release. The value of  $dI_{SXR}/dt$  had its maximum near the time of spike 4. Though SXR intensity achieved its maximum at 20:48-20:49, there were small positive values of  $dI_{SXR}/dt$  after the 20:49 interval up to 20:52. This fact indicates that some energy input should be present in the SXR radiating volume during this time.

The counting rate in the channels below 750 keV during the time interval of the main energy release (spikes 1-5) was  $\sim 1.7$  times higher than in spike 6. The same is true for the ratio of the radio waves intensities at 15.4 GHz. In addition, shifting the frequency of spectral maximum from 15.4 GHz at the time of spikes 4-5 to the 4.995 GHz at spike 6 can indicate a density decrease in the region of electron trapping. It seems also that ‘‘Neupert law’’ is not valid directly during this time interval because the SXR derivative does not exceed 0.1 of its maximum value. Presumably this episode of particle acceleration took place in another, larger region than the main energy release of the flare.

Let us now discuss the high-energy band of gamma emission observed by SONG. Magnitudes of the count rate in spikes 1-5 and in interval 6, are leveled off in three channels between energies 0.75–10.5 MeV (see panels f, g). Flare emission in the 10 MeV–22.5 MeV range started to rise at about 20:44-20:45 UT. At energies above 22.5 MeV a statistically significant flare emission was observed after 20:47 (panels g, i). Its intensity peaked at 20:48–20:51, before the maximum time of spike 6.

The bottom panel of the Figure shows the time dependence of the distance between HXR FPs. The FPs firstly moved toward and then away from each other. The transition from the contracting of conjugate FPs to the onset of movement apart is denoted by the vertical sparse area. The transition between these two phases of FP motions coincided with the beginning of spikes 4 and 5 and with the appearance of high-energy emission at the energies  $>10.5$  MeV. In fact, we see that the conditions of particle acceleration changed somehow at this time.

In order to trace the time evolution of the electron and proton acceleration efficiency, we restored the emission spectra at successive time intervals. In addition, we restored the spectra of several distinct narrow spikes 2 and 3, 4 and 5.

### 3. The dynamics of the flare gamma-ray emission spectrum

Our measurements allow us to restore gamma-ray emission spectra of a flare. In the flare under study we used a three-component model of the flare spectrum: (1) the bremsstrahlung from primary accelerated electrons; (2) a line spectrum from nuclear de-excitation; and (3) the broad continuum produced by pion decay.

The bremsstrahlung spectrum is described as a power law with roll-over at high energies:

$$F(E) = I_0 E^{-\gamma} \exp\left(-\frac{E}{E_0}\right). \quad (1)$$

Energy resolution of the CsI crystal and broad energy channels of SONG did not allow us to separate discrete narrow gamma-lines. That is why we consider integrated deposit from these lines to the SONG count rate in the energy range of 0.5–12 MeV and use in our fitting a broad continuum produced by prompt lines. A shape of the continuum was obtained from Figure 20 of Murphy et al. (2009). We did not include the delayed line 2.225 MeV in the model because the width of this line is 25 keV, so its contribution to the total count rate of the SONG channel of 2-6 MeV is negligible.

The pion-decay continuum consists mainly of the wide gamma line peaking at 67 MeV, produced by neutral-pion decay and bremsstrahlung generated by secondary positrons. This spectrum component was calculated by R. Murphy and kindly provided to us (private communication). It is, in general, similar to a typical shape of this continuum (see, e.g., Figure 18 in Murphy et al., 1987).

The response functions of the SONG detector were simulated separately for spectrum components considered above with the help of the GEANT 3.21 program. Then we fitted recorded count rates and found weights of different components. Figure 2 shows the emission spectra restored from the SONG data accumulated in the 9 successive time intervals. We also insert in this Figure spectra obtained from the RHESSI data in the energy range of 0.1–10 MeV. These spectra were restored separately for front and rear segments of the detector (Lin et al., 2002) using the standard package for data processing in the RHESSI Solarsoft for IDL (<http://www.lmsal.com/solarsoft/>). The RHESSI fluxes exceed distinctly the SONG ones at 20:47–20:52 UT (see panels d-f), which could be due to contamination by charged particles into count rates of the RHESSI detectors.

Note that RHESSI detectors have no anticoincidence shield and possibility of this contamination from radiation belt particles was previously reported by Hurford et al. (2006) and Liu et al. (2009). In spite of the difference of models used for the spectra restoration from the SONG and RHESSI data, a good agreement between these spectra is seen during non-contaminated time intervals that proves the correctness of the restored spectra.

The flare under consideration exhibits various temporal characteristics of components created by electrons and protons with different energies. Figure 2 demonstrates that:

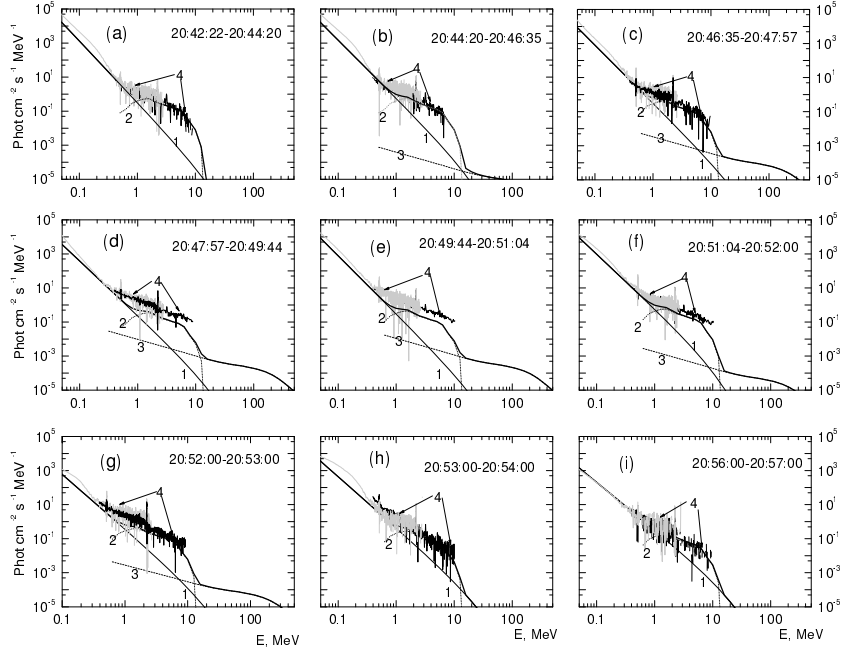


**Figure 2.** HXR and gamma-emission spectra of the 29 October 2003 flare in 9 time intervals. The SONG total spectrum is shown by a thick black line; spectral components are numbered as follows: bremsstrahlung - 1, the gamma-line continuum - 2, and the pion-decay emission - 3. The spectra measured by RHESSI (4) are shown by gray (frontal segments) and black curves (rear segments).

1. The electron bremsstrahlung spectrum extended up to 10–15 MeV from the very beginning of the flare impulsive phase. It means that at this time the electrons were accelerated at least to the same energies. Parameter  $\gamma$  describing hardness of the bremsstrahlung continuum spectrum, is presented in Table 1. During the FP contracting flare phase, the softest spectrum, with  $\gamma$  equal to 4.4, was at the very beginning of the flare. Later on,  $\gamma$  became equal to 3.8-3.6. In the phase when FPs moved away from each other the spectrum became harder and did not change, remaining equal to  $3.4 \pm 0.2$ . There is spectrum hardening at the very end of the flare after 20:53. Spectrum hardening is explained if electrons with low energies were escaping from the trap faster than high energy ones due to scattering.
2. Fluxes at 2-10 MeV are mainly produced by narrow gamma-line emission because this emission was at least ten times more intense than the electron bremsstrahlung. These lines appeared also at the very beginning of the flare

and presented in all spectra, suggesting that protons were accelerated up to 10–50 MeV at this time and later on.

3. Fluxes at energies above 10 MeV appeared after  $\sim 20:44:20$  UT, and they represent the pion-decay emission entirely, because the electrons bremsstrahlung was vanishing near 10–20 MeV.

#### 4. Estimate of accelerated proton spectrum

The three-component spectrum model allows us to make straightforward estimates of a different component intensity that permits to study separately the time evolution of these components. For further analysis we calculated fluences of each component from the restored spectra. The gamma-line flux was summed over the 4–7 MeV range, the pion-decay emission flux over the 30–100 MeV range, and the total bremsstrahlung flux at energies  $>100$  keV. Time behaviors of these components are presented in Table 1.

The ratio  $R$  of pion-decay emission and gamma-lines intensities depends strongly on the shape of the accelerated-particle spectrum because these components are produced by particles belonging to different energy ranges of a parent proton spectrum (Ramaty and Murphy, 1987). An expected  $R$  value can be calculated under certain assumptions on the proton spectrum and spatial distribution, as well as on chemical abundance of the solar atmosphere, and vice versa: the proton spectrum shape can be estimated from this ratio obtained experimentally. We calculated this ratio  $R$  from the restored spectra (see Table 1). Then we determined parameters of parent proton spectra using Figure 4 from Dunphy et al. (1999). The latter Figure presents calculated values of  $R$  for a power-law spectrum  $N_p(E) = I_0 E^{-S}$  versus the index  $S$ . The values of  $S$  found this way are presented in Table 1.

The number of protons with energies  $>30$  MeV strongly depends on the chosen fitting model and its parameters (see, e.g., Murphy et al., 1987; Vilmer et al., 2003). In other words, it depends on the pion-decay component intensity and on ambiguity of our knowledge of the real spectral shape – a power law with various spectral indices  $S$ , or an exponential. The total proton number with energies above 30 MeV was estimated for a power law proton spectrum with indices given in Table 1. The results are presented in the last column of Table 1.

#### 5. Time evolution of the efficiency of acceleration of protons and electrons

We examined temporal evolution of the efficiency of protons acceleration processes with respect to processes of electron acceleration. The gamma-line flux,

Table 1. HXR and gamma-ray component fluxes and parameters of parent proton spectra

UT	$\gamma$	Flux, phot cm <sup>-2</sup> s <sup>-1</sup>		R	S	$N_p$ (>30 MeV)
		Bremsstr. 100 keV	$\gamma$ -lines, 4-7 MeV			
1	20:40:36-20:41:10	2.1 10 <sup>1</sup>	7.3 10 <sup>-2</sup>	-	-	-
2	20:41:10-20:42:22	2.9 10 <sup>1</sup>	1.9 10 <sup>-1</sup>	-	-	-
3	20:42:22-20:44:20	6.7 10 <sup>1</sup>	4.1 10 <sup>-1</sup>	<1.4 10 <sup>-3</sup>	>4.7	-
4	20:44:20-20:46:35	8.0 10 <sup>1</sup>	4.2 10 <sup>-1</sup>	(8.8±5.5) 10 <sup>-4</sup>	4.6	2.1 10 <sup>31</sup>
5	20:46:35-20:47:51	4.3 10 <sup>1</sup>	3.1 10 <sup>-1</sup>	(7.5±5.1) 10 <sup>-3</sup>	4.0	2.8 10 <sup>31</sup>
6	20:47:51-20:49:44	2.2 10 <sup>1</sup>	2.6 10 <sup>-1</sup>	(2.2±0.5) 10 <sup>-2</sup>	3.7	6.1 10 <sup>31</sup>
7	20:49:44-20:51:04	4.2 10 <sup>1</sup>	3.4 10 <sup>-1</sup>	(2.5±0.6) 10 <sup>-2</sup>	3.7	6.4 10 <sup>31</sup>
8	20:51:04-20:52:00	5.5 10 <sup>1</sup>	4.5 10 <sup>-1</sup>	(4.0±2.3) 10 <sup>-3</sup>	4.2	1.9 10 <sup>31</sup>
9	20:52:00-20:53:00	3.4 10 <sup>1</sup>	3.0 10 <sup>-1</sup>	(6.3±2.6) 10 <sup>-3</sup>	4.0	2.0 10 <sup>31</sup>
10	20:53:00-20:54:00	2.7 10 <sup>1</sup>	2.1 10 <sup>-1</sup>	-	-	-
11	20:54:00-20:55:00	2.5 10 <sup>1</sup>	1.9 10 <sup>-1</sup>	(3.0±6.0) 10 <sup>-3</sup>	1.6 10 <sup>-2</sup>	1.1 10 <sup>31</sup>
12	20:55:00-20:56:00	2.2 10 <sup>1</sup>	1.7 10 <sup>-1</sup>	-	-	-
13	20:56:00-20:57:00	1.4 10 <sup>1</sup>	1.4 10 <sup>-1</sup>	-	-	-

being a signature of interactions of ions with energies of tens of MeV, was compared with an electron bremsstrahlung profile. First of all, we investigate the individual spikes numbered as 2, 3, 4 and 5 in Figures 1 and 3(a). Figure 3, panels (b, c), shows the emission spectra restored from the SONG data accumulated in the time of these spikes. Figure 3 shows e spectra of these spikes.

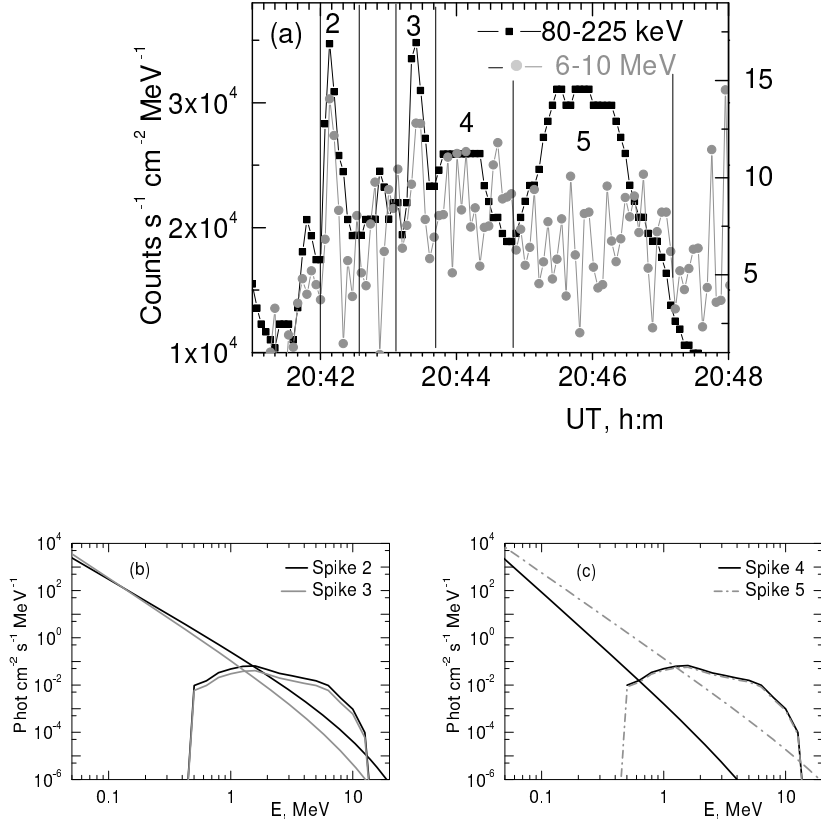


**Figure 3.** Panel a - time profiles of the count rate in the channels 80–225 keV and 6–10.5 MeV with 4-s time resolution. Thin vertical lines indicate the time interval of each spike. HXR and gamma-emission spectra in separated spikes 2, 3, (panel b) and in 4,5 (panel c). Each spectrum was obtained after subtracting the count rate of the smoothed trend of SONG channels.

The results of spectra restoration of these spikes are presented in Table 2.

Figure 3 (panels b, c) demonstrates that the narrow gamma-line emission was considerably more intense than the electron bremsstrahlung during each

**Table 2.** HXR and gamma-ray component fluxes

No. spike	Time	$\gamma$	$E_0$ MeV	Flux, phot cm <sup>-2</sup> s <sup>-1</sup>		$\gamma$ -lines/ Bremsstr. ratio
				Bremsstr. >100 keV	$\gamma$ -lines, 4-7 MeV	
2	20:42:00-20:42:34	3.0	5	1.85 10 <sup>1</sup>	4.9 10 <sup>-2</sup>	0.0026
3	20:43:16-20:43:43	3.2	3	1.8 10 <sup>1</sup>	3.1 10 <sup>-2</sup>	0.0017
4	20:43:43-20:44:39	4.6	3	3.5 10 <sup>0</sup>	4.1 10 <sup>-2</sup>	0.012
5	20:44:46-20:47:10	3.6	20	2.9 10 <sup>1</sup>	4.3 10 <sup>-2</sup>	0.0015

spike. Therefore, the behavior of the count rate in the channel 6-10.5 MeV can be considered as the time evolution of proton acceleration. So we can compare time behavior of the count rate of this channel with the count rate of the channel 80-225 keV that reflects the efficiency of electron acceleration. It is seen (panel a) that protons were accelerated up to 30-50 MeV simultaneously with electrons in each spike within 4-s time resolution. Table 2 shows that:

- proton acceleration efficiency relative to the efficiency of electron acceleration increased considerably in spike 4 (20:43:43-20:44:39) when compared with others spikes. Let us recall that this short considerable increase occurred in the short transition of FP motion at 20:44:20-20:45;
- the spectrum of accelerated electrons was hardest during the spike 2.

Next, we examined temporal evolution of the efficiency of protons acceleration processes comparing with the process of electron acceleration during the whole flare impulsive phase (Figure 4, panel a). There is a marginally different increase in this ratio during the flare phase when FPs are moving away from each other.

The pion-decay flux is a signature of interaction of ions with energies above 300 MeV. The temporal behavior of the pion-decay component (also presented in panel a) matched the temporal behaviors of this ratio. Panel c shows that the proton spectrum index  $S$  was hardest during this time. We presented time variations of the reconnection electric field (panel d) calculated by Yang et al. (2011) from HXR (RHESSI) and UV ribbons (TRACE) observations. In spite of the gap of the data in the most interesting time, the second growth in the reconnected electric field near the time of the greatest efficiency of the proton acceleration can be seen.

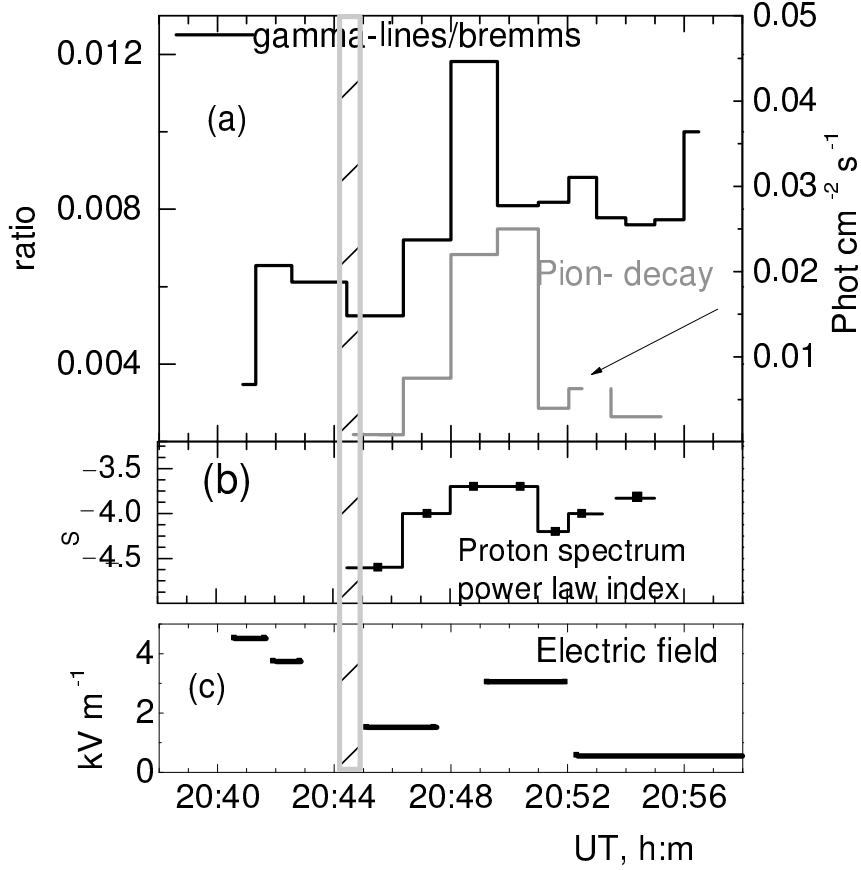


**Figure 4.** Upper panel-a: the ratio of the gamma-line flux to the bremsstrahlung one (black line, left scale), the pion-decay time profile (gray line, right scale). The estimated spectrum index  $S$  of parent protons (panel b). Estimated electric field (taken from Yang et al., 2011) presented at the bottom panel c.

## 6. Application of the results of the pion-decay emission observations to investigation of GLE

Observation of the flare pion-decay emission can provide reliable information on acceleration time of protons responsible for a GLE. A certain fraction of protons accelerated during a flare moves downward, interacts with the solar atmosphere and produces the observed gamma emission. Another proton fraction escapes the Sun and can produce a GLE. The cross section of pion production increases

rapidly from the threshold (300 MeV) to about 1 GeV, and then continues to increase slowly. Hence, the pion-decay emission is generated mainly by protons with energies typical for a GLE above 1 GeV. Therefore, it is possible and useful to compare time scales of these processes (Kurt et al., 2010b).

The flare that occurred on 29 October 2003 was accompanied by GLE 66. Figure 5 presents the observed time profile of the pion-decay gamma-emission that reproduces time evolution of protons' population accelerated at the Sun, and the data of three NMs which recorded the earliest GLE onset.

The cut-off rigidity for the Newark NM is equal to  $R_c = 2.09$  GV and for the Sanae NM to 1.1 GV. The energy of protons observed by the South Pole NM is above 400 MeV due to the atmospheric absorption.

During this event the time lag between the pion-decay emission observation and the GLE onset was equal to 12–14 minutes if protons were accelerated simultaneously with the pion-decay emission appearance, or to 9–10 minutes if this acceleration operated during the time interval of the maximum intensity of the pion-decay emission.

## 7. Summary and Conclusions

The particle acceleration up to sub-relativistic energies plays an important role in a large flare/CME event. As it is mentioned in the introduction, it is still not clear whether this acceleration is initiated by CME/fast shock - wave propagation in the lower corona, or it occurred during the process of a fundamental restructuring of the flare magnetic field.

We presented results of CORONAS/SONG observations of high-energy electromagnetic emissions during the bulk of the 29 October 2003 solar flare duration in the 40 keV–150 MeV energy range and compared these data with other observational manifestations of the flare. We restored incident spectra of flare emission using the three-component spectrum model and traced the temporal evolution of different components. We also restored the flare emission spectra from the RHESSI data and found a good agreement between the SONG and RHESSI spectra in the energy range of 0.1–10 MeV. We found that electrons were accelerated up to 10 MeV and protons generating gamma-lines up to 10–50 MeV since the very beginning of the flare. We estimated the accelerated proton spectrum using the ratio of fluxes of the pion-decay emission and gamma-lines, and found that this spectrum was changing during the flare course. The hardest spectrum ( $S = 3.7$  for a power law) was at 20:46:37–20:53 UT. Similar estimates have been performed so far only for 1982 June 03 (Ramaty and Murphy, 1987; Murphy et al., 1987) and 1991 June 11 flares (Dunphy et al., 1999).

We have treated the time behavior of the proton acceleration up to energies of pion-decay production. We can assert with certainty that the pion-decay emission appeared between 20:46:35 and 20:47:51. Note that the onset time of the shock wave-induced type II radio emission was observed at 20:42 UT, i.e.

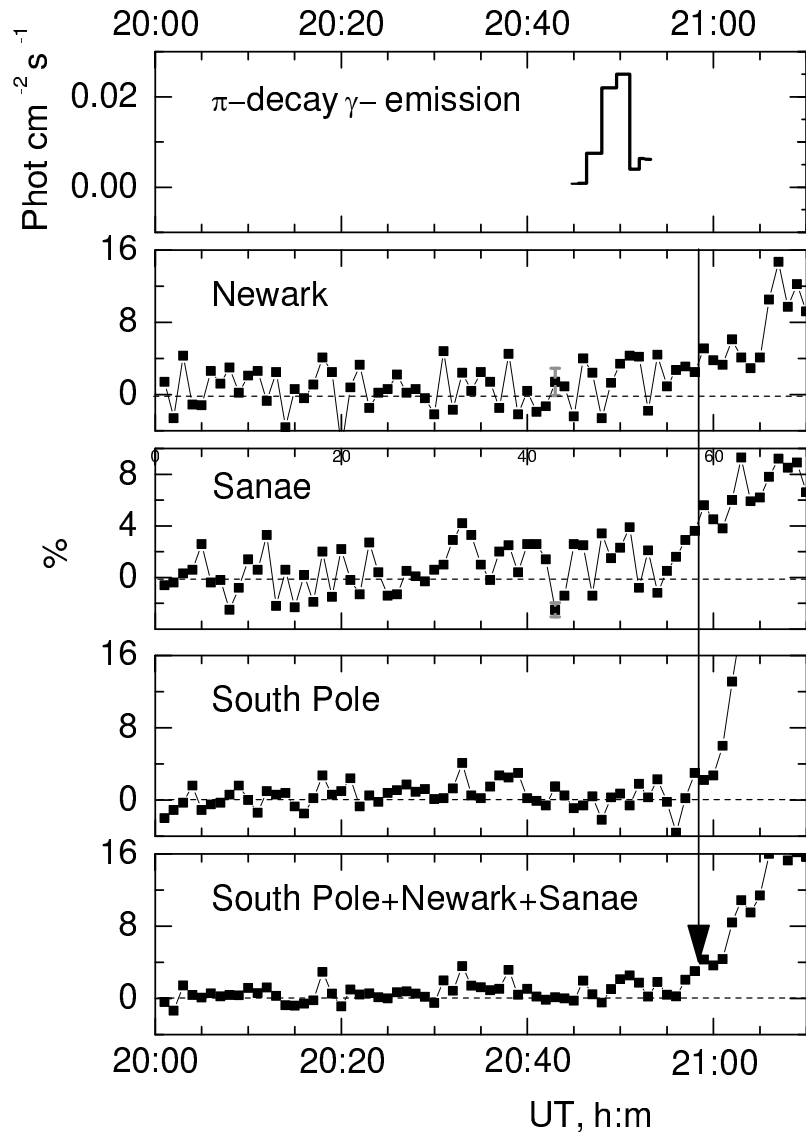


**Figure 5.** The pion-decay gamma-emission observed by SONG (panel a) and relative count rates of selected NMs (panels b-d) and their sum (panel e). The vertical arrow marks the GLE onset.

near the flare onset. This time difference makes hard to explain the proton acceleration by the action of a shock wave. On the other hand, a significant change of the flare magnetic field structure during the development of this flare was discovered (see, e.g. Ji et al., 2008; Liu et al., 2009; Zhou et al., 2008; Xu et al., 2010; Yang et al., 2011). A two phase reconfiguration of flare magnetic field (visible, in particular, in motion of the conjugate HXR foot points/UV kernels) was found. Various possible magnetic reconnection scenarios were proposed in these papers; in particular Ji et al. (2008) supposed that the flare evolves from a sigmoid to an arcade phase. This transition between the two phases coincided with the subdivision of the flare based on SONG observations of the high-energy X-ray and gamma-ray emissions. It seems that protons accelerated to high energies appeared in the solar atmosphere simultaneously, or near the time of this magnetic field reconnection. Thus, it is worthwhile to discuss the relationship between the reconnection electric field and the acceleration of electrons and protons. It is usually assumed that the electron acceleration is caused directly by the reconnection electric field. The lower panel of Figure 4 represents the calculated electric field during several time intervals (Yang et al., 2011). Despite the gap in the data, it is seen that the two peaks visible in the electric field are close to the phases of particle acceleration (20:38-20:44:20 and 20:44:20-20:53, respectively).

We showed that the efficiency of the electron acceleration process was weaker in the second period when compared with the first one. By contrast, the proton acceleration became most effective at this time, implying that other acceleration mechanisms became important in the late phase when the magnetic field structure fundamentally changed.

The 29 October 2003 flare occurred in the large super-active region NOAA 10486. The pion-decay gamma-emission flux was equal to  $2.2 \cdot 10^{-4}$  at 100 MeV. The maximum of the hard X-ray emission flux at 100 keV was about  $1.5 \cdot 10^3$  phot  $\text{cm}^{-2} \text{s}^{-1} \text{MeV}^{-1}$ . Compare these values with the fluxes of a major flare of X18 importance on 28 October that occurred in the same active region. The pion-decay flux was 50 times higher than the flux observed in the flare on 29 October 2003. At the same time, the maximum of the electron flux was only 6 times higher (Kuznetsov et al., 2011).

This event was accompanied by GLE 66. We compared the time of the pion-decay gamma-emission maximum with the GLE onset and found that the time lag between the pion-decay emission observation and the GLE onset was equal to 12–14 minutes if protons were accelerated simultaneously with the pion-decay emission appearance. If this acceleration operated during the time interval of maximum intensity of the pion-decay emission, it was equal to 9–10 minutes. Previously, we found that the first particles responsible for GLE 66 and 69 onset reached 1AU a few minutes after the pion-decay emission was observed (Kurt et al., 2010b; 2013b,c). This time lag corresponds to the particle propagation time from the Sun to the Earth under the following assumptions: the first GLE particles escape the Sun immediately after acceleration, propagate almost without

scattering, and belong to the same population of accelerated particles that produce the pion-decay emission. Note that this lag depends strongly on the length of the interplanetary magnetic field (IMF) line. The reasons of a relatively long delay of the GLE 66 onset can be the location of the considered flare of 29 October 2003 (W05), or the very disturbed conditions of interplanetary space during the passage of region NOAA 10486 across the solar disk (Veselovsky et al., 2004). In this case, one cannot assume a regular structure of the IMF and, in particular, to evaluate the length of the Archimedean spiral. Likewise in this case, the real velocity of the particles could be reduced by 1.3-1.5 times as compared to their ‘kinetic’ velocity.

Everything stated above, including early time of the occurrence of the shock wave, suggests that this lag between the appearance of protons accelerated to high energies in the solar atmosphere and the GLE onset does not contradict the assumption that particles responsible for the GLE beginning were accelerated at the Sun simultaneously with the particles generating the pion-decay emission. In other words, they both can belong to the same population of accelerated particles.

**Acknowledgements.** Authors would like to thank A.V Belov for providing NM worldwide network data and KK to VEGA 2/0040/13. The reviewer is acknowledged for his/her important comments.

## References

- Ackermann, M., Ajello, M., Allafort, A., et al.: 2012, *Astrophys. J.* **745**, 144  
 Ackermann, M., Ajello, M., Albert, A., et al.: 2014, *Astrophys. J.* **787**, 15  
 Akimov, V.V., Afanassyev, V.G., Belousov, A.S., et al.: 1991, in *Proc. 22nd Int. Cosmic Ray Conf.*, The Institute for Advanced Studies, Dublin, **3**, 73  
 Akimov, V.V., Ambroz, P., Belov, A.V., et al.: 1996, *Sol. Phys.* **166**, 107  
 Alexander, D., Dunphy, P.P., McKinnon, A.L.: 1994, *Sol. Phys.* **151**, 147  
 Chupp, E.L., Debrunner, H., Flückiger, E. et al.: 1987, *Astrophys. J.* **318**, 913  
 Chupp, E.L., Trotter, G., Dunphy, P.P., Rieger, E.: 2003, in *Proc. 28th Int. Cosmic Ray Conf.*, Tsukuba, 3171  
 Chupp, E.L., Ryan, J.M.: 2009, *Res. Astron. Astrophys.* **9**, 11  
 Debrunner, H., Lockwood, J.A., Barat, C., et al.: 1997, *Astrophys. J.* **479**, 997  
 Dennis, B.R., Zarro, D.M. 1993, *Sol. Phys.* 146, 177  
 Dennis, B.R., Veronig, A., Schwartz, R.A., et al.: 2003, *Adv. Space Res.* **32**, 2459  
 Dunphy, P.P, Chupp E.L., E.Rieger 1990, in *Proc. 21st Int. Cosmic Ray Conf.*, Adelaide, **5**, 75  
 Dunphy, P.P, Chupp, E.L.: 1991, in *Proc. 22nd Int. Cosmic Ray Conf.*, Dublin, **3**, 65  
 Dunphy, P.P., Chupp, E.L., Bertsch, D.L., et al.: 1999, *Sol. Phys.* **187**, 45  
 Forrest, D.J., Vestrand, W.T., Chupp, E.L., et al.: 1985, in *Proc. 19th Int. Cosmic Ray Conf.* La Jolla, **4**, 146  
 Forrest, D.J., Vestrand, W.T., Chupp, E.L., et al.: 1986, *Adv. Space Res.* **6**, 115  
 Hudson, H.S.: 1991, *Bull. Am. Astron. Soc.* **23**, 1064  
 Hurford, G.J., Krucker, S., Lin, R.P., et al.: 2006, *Astrophys. J.* **644**, L93

- Ji H., Wang H., Lui C., Dennis B.R.: 2008, *Astrophys. J.* **680**, 734
- Kurt, V.G., Yushkov, B.Yu., Kudela, K., Galkin, V.I.: 2010a, *Cosmic Res.* **48**, 70
- Kurt, V.G., Yushkov, B.Yu., Belov, A.V.: 2010b, *Astron. Lett.* **36**, 520
- Kurt, V.G., Kudela, K., Yushkov, B.Yu., Galkin, V.I.: 2013a, *Adv. Astron.*, paper 690921.
- Kurt, V., Yushkov, B., Belov, A., et al.: 2013b, *J. Phys.: Conf. Ser.* **409**, paper 012151
- Kurt, V.G., Yushkov B.Yu., et al.: 2013c, *Bull. Russian Acad. Sci.: Physics* **77**, 483
- Kuznetsov S.N., Kudela K., Myagkova I.N., et al.: 2004, *Indian J. Radio Space Phys.* **33**, 353
- Kuznetsov, S.N., Kurt, V.G., Yushkov, B.Yu., Kudela, K., et al.: 2011, *Sol. Phys.* **268**, 175
- Lin R.P., Dennis B.R., Hurford G.J., et al.: 2002, *Sol. Phys.* **210**, 3
- Liu W., Petrosian V., Dennis B.R., Holman G.D.: 2009, *Astrophys. J.* **693**, 847
- Miller J.A., Ramaty, R.: 1989, *Astrophys. J.* **344**, 973
- Murphy, R.J., Ramaty, R.: 1984, *Adv. Space Res.* **4**, 127
- Murphy, R.J., Dermer, C.D., Ramaty, R.: 1987, *Astrophys. J., Suppl. Ser.* **63**, 721
- Murphy, R.J., Kozlovsky B., Kiener, J., Share, G.: 2009, *Astrophys. J., Suppl. Ser.* **183**, 142
- Marschhäuser, H., Rieger, E., Kanbach, G.: 1991, in *Proc. 22nd Int. Cosmic Ray Conf.*, Dublin, **3**, 61
- Neupert, W.M.: 1968, *Astrophys. J.* **153**, L59
- Ramaty, R., Murphy, R.J.: 1987, *Space Sci. Rev.* **45**, 213
- Rank, G., Ryan, J.M., Debrunner, H., et al.: 2001, *Astron. Astrophys.* **378**, 1046
- Rieger, E., Marschhäuser, H.: 1991, in *Max '91/SMM Solar Flares: Observations and Theory*, eds.: Winglee, R.M., Kiplinger, A.L., 68
- Schneid, E.J., Bertsch, D.L., Dingus B.L., et al.: 1996, *Astron. Astrophys., Suppl. Ser.* **120**, 299
- Schrijver, C.J., Hudson, H.S., Murphy, R.J., et al.: 2006, *Astrophys. J.* **650**, 1184
- Terekhov, O.V., Sunyaev, R.A., Tkachenko, A.Yu., et al.: 1996, *Astron. Lett.* **22**, 143
- Veselovsky, I.S. et al.: 2004, *Cosmic Res.* **42**, 433
- Vestrand, W.T., Share, G.H., Murphy, R.J., et al.: 1999, *Astrophys. J., Suppl. Ser.* **120**, 409
- Vilmer, N.: 1994, *Astrophys. J., Suppl. Ser.* **90**, 611
- Vilmer, N., MacKinnon, A.L., Hurford, G.J. 2011, *Space Sci. Rev.* **159**, 167
- Xu, Y., Jing, J., Cao, W., Wang, H.: 2010, *Astrophys. J.* **709**, L 142–L145
- Yang, Y.-H., Cheng, C.Z., Krucker, S., Hsieh, M.-S.: 2011, *Astrophys. J.* **732**, 15
- Zhou T.-H., Ji H.-S., Huang G.: 2008, *Adv. Space Res.* **41**, 1195